Monte Carlo Analysis of Obstructed Diffusion in Three Dimensions: Application to Molecular Diffusion in Organelles

Bence P. Ölveczky and A. S. Verkman
Departments of Medicine and Physiology, Cardiovascular Research Institute, University of California, San Francisco, California 94143 USA

ABSTRACT Molecular transport in the aqueous lumen of organelles involves diffusion in a confined compartment with complex geometry. Monte Carlo simulations of particle diffusion in three dimensions were carried out to evaluate the influence of organelle structure on diffusive transport and to relate experimental photobleaching data to intrinsic diffusion coefficients. Two organelle structures were modeled: a mitochondria-like long closed cylinder containing fixed luminal obstructions of variable number and size, and an endoplasmic reticulum-like network of interconnected cylinders of variable diameter and density. Trajectories were computed in each simulation for $>10^5$ particles, generally for $>10^5$ time steps. Computed time-dependent concentration profiles agreed quantitatively with analytical solutions of the diffusion equation for simple geometries. For mitochondria-like cylinders, significant slowing of diffusion required large or wide single obstacles, or multiple obstacles. In simulated spot photobleaching experiments, a ~25% decrease in apparent diffusive transport rate (defined by the time to 75% fluorescence recovery) was found for a single thin transverse obstacle occluding 93% of lumen area, a single 53%-occluding obstacle of width 16 lattice points (8% of cylinder length), 10 equally spaced 53% obstacles alternately occluding opposite halves of the cylinder lumen, or particle binding to walls (with mean residence time = 10 time steps). Recovery curve shape with obstacles showed long tails indicating anomalous diffusion. Simulations also demonstrated the utility of measurement of fluorescence depletion at a spot distant from the bleach zone. For a reticulum-like network, particle diffusive transport was mildly reduced from that in unobstructed three-dimensional space. In simulated photobleaching experiments, apparent diffusive transport was decreased by 39–60% in reticular structures in which 90–97% of space was occluded. These computations provide an approach to analyzing photobleaching data in terms of microscopic diffusive properties and support the paradigm that organellar barriers must be quite severe to seriously impede solute diffusion.

INTRODUCTION

Intracellular signaling and metabolism involve the diffusive transport of metabolite- and enzyme-sized solutes in cell aqueous compartments. It has been proposed that solute diffusion in the mitochondrial matrix is an important determinant of metabolic rates. In the aqueous lumen of the endoplasmic reticulum and Golgi, diffusion of nascent protein may be important for interactions with the protein folding machinery and with enzymes that carry out post-translational modifications. Photobleaching measurements have quantified the diffusional mobility of small solutes (Kao et al., 1993) and macromolecule-size solutes (Luby-Phelps et al., 1987; Swaminathan et al., 1997; Seksek et al., 1997) in cytoplasm, and various methods have been used to study the motion of larger structures in the nucleus such as chromatin (Lang et al., 1986; Alexander and Rieder, 1991; Shelby et al., 1996; Seksek et al., 1997; Abney et al., 1997). Recently, diffusion was measured in small intracellular organelles by photobleaching of green fluorescent protein (GFP) in the aqueous matrix of mitochondria (Partikian et al., 1998), the aqueous lumen of endoplasmic reticulum (Dayel and Verkman, 1998), and the limiting membrane of Golgi (Cole et al., 1996). The targeting of GFP to specific intracellular locations (Rizzuto et al., 1995; DeGiorgi et al., 1996) now permits measurements of diffusion in many organellar compartments.

There are several important issues in the analysis of solute diffusion in organellar compartments. Organelles often have a complex exterior geometry as well as internal barriers. For example, the mitochondrial matrix is generally seen by electron microscopy as a cylindrical compartment with internal cristae, as shown schematically in Fig. 1 *A* (Srere, 1980; Halestrap, 1989). The endoplasmic reticulum is generally thought of as an interconnected reticular network of cylinders or flat ribbons/plates in three dimensions (Fig. 1 *B*). From a practical experimental perspective, a strategy is needed to deduce intrinsic solute diffusion coefficients (for diffusion in the absence of boundaries or barriers) from measured photobleaching recovery or depletion data. A more general issue is the elucidation of how organellar shape and barrier geometry influence particle diffusion in vivo. For example, how do cristae barriers affect the diffusional transport of metabolites along the mitochondrial axis? Does a continuously open reticular network dramatically slow long-range diffusive transport?

The computational analysis reported here was done to evaluate the influence of organelle geometry on solute diffusion in three dimensions. Although theoretical descriptions of particle diffusion in two-dimensional membranes have been reported for a variety of situations involving

Received for publication 6 November 1997 and in final form 26 January 1998.

Address reprint requests to Dr. Alan S. Verkman, Cardiovascular Research Institute, 1246 Health Sciences East Tower, Box 0521, University of California–San Francisco, San Francisco, CA 94143-0521. Tel.: 415-476-8530; Fax: 415-665-3847; E-mail: verkman@itsa.ucsf.edu.

© 1998 by the Biophysical Society

0006-3495/98/05/2722/09 $2.00

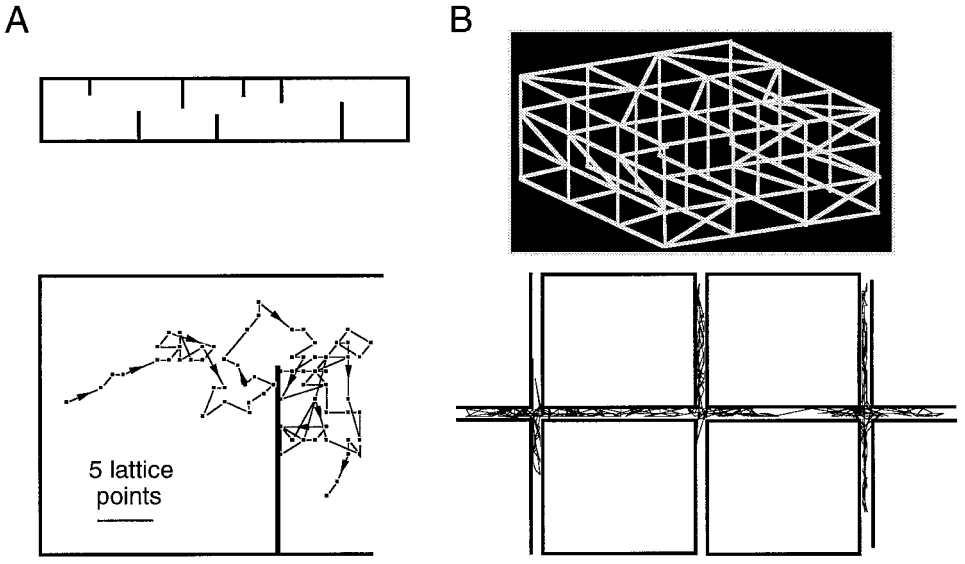

FIGURE 1 Schematic representation of a mitochondrion (*A*) as a long cylinder with internal obstructions, and of endoplasmic reticulum (*B*) as a 3-D array of interconnected cylinders with continuously open lumen (shown in *white*) in which particle diffusion occurs. Bottom: Computer-generated random walks in which the particle position at every 10th time point is shown. Trajectories are shown as 2-D projections of 3-D random walks. See text for details.

binding, crowding (Scaletter and Abney, 1991), and mobile and immobile obstacles (Saxton, 1990; Schram et al., 1994), computations have not been made for aqueous-phase particle diffusion in three dimensions for organellar geometries. We have utilized random walk simulations in three dimensions to analyze the effects of barrier properties on diffusion in mitochondria and the effects of reticular geometry on diffusion in endoplasmic reticulum. Computations were carried out to describe in vivo solute diffusion and to relate experimental photobleaching data to intrinsic particle diffusion coefficients.

METHODS

Diffusion in three dimensions was modeled as a random walk process, in which the diffusing particles move on a cubic lattice that was restricted in space to correspond to the specified organelle structure. Mitochondria were modeled as cylinders of length 200 lattice points and diameter 20 lattice points. A plane perpendicular to the axis of the cylinder thus contained 317 lattice points. The endoplasmic reticulum was modeled as a 3-D orthogonal grid made up of connected cylinders. The extent of the orthogonal grid was infinite in the x,y plane and finite in the z direction. The cylinders making up the reticulum had a specified diameter and spacing, resulting in occlusion of 90–99% of 3-D space. We chose to model the endoplasmic reticulum as a network of cylinders rather than of plates because cylinders represent an extreme situation in which solute diffusion might be most slowed. For each time step in the random walk, a particle had two options to move to an adjacent lattice point along each of the three orthogonal axes (e.g. $-x$ or $+x$). A pseudorandom number, generated using L'Ecuyer's method with Bays-Durham shuffle and added safeguards to ensure randomness (Press et al., 1992), was used to determine which of the six adjacent sites the particle moved to. Because each random walk trajectory was independent, there was no interaction between the traced particles, allowing each of the particles to move to any of its six neighboring lattice points.

In the mitochondrial simulations, the obstacles representing the cristae were defined as continuous thin barriers (zero width) located between two lattice planes perpendicular to the axis of the cylinder and occluding a specified percentage of the cross-sectional area. In some simulations the barriers were specified with finite width (along the cylinder axis) or other geometries. Simulations were carried out to investigate diffusive transport in the presence of single obstacles of defined shape and size, as well as the effect of a series of equally spaced cristae along the length of the mitochondria. When, during a random walk, a particle was to be moved across a barrier or a boundary, the particle remained in place, equivalent to its being reflected by the obstacle. Particle binding to cylinder walls and barriers was modeled in some simulations by defining a mean residence time in which the particle remained in situ if it collided with a barrier or boundary.

To simulate fluorescence photobleaching recovery and fluorescence depletion (decrease in fluorescence at a region different from the bleach zone) experiments, the initial particle distribution was taken as the volume of the organelle that intersects a cylindrical beam (simulating the bleach beam) of specified radius. The time-resolved concentration of particles in the bleach volume was then used to generate fluorescence recovery curves. Fluorescence depletion curves were computed from the time-resolved concentration in a specified volume distant from the bleach zone. In general, random walk trajectories for $>10^5$ particles were computed for each simulation. Simulations using greater spatial resolution (lattice resolution increased by a factor of 10 with cylinder size constant) did not affect concentration profiles or simulated photobleaching curves, apart from producing smoother data. The number of time steps for each run (generally 65,000–200,000) was chosen so that particle concentration along the cylinder was nearly constant at the end of the calculations. For the reticulum simulation the number of time steps was chosen to give >95% complete fluorescence recovery.

To validate the results, the 3-D random walk simulation for a finite cylinder without barriers was compared to the 1-D analytic solution of the diffusion equation. The solution to the diffusion equation for a cylinder of length $2L$, where particles are initially in a narrow (delta function) plane located a distance ϵ away from the center, is (Partikian et al., 1998)

$$C(x, t, \epsilon) = M(4\pi Dt)^{-1/2}e^{-(x-\epsilon)^2/4Dt} + \sum_{n=1}^{\infty} M(4\pi Dt)^{-1/2}\left[e^{-(x-2nL+\epsilon)^2/4Dt} + e^{-(x+2nL+\epsilon)^2/4Dt}\right] \quad (1)$$

where M is related to the number of particles and D is the diffusion coefficient. If instead the particles are initially in a uniform distribution between planes at $\epsilon - h$ and $\epsilon + h$ (simulating initial conditions of photobleaching experiment), the solution to the diffusion equation

becomes

$$C(x, t, \epsilon) = C_0\left[0.5\left(\operatorname{erfc}\left(\frac{x-h-\epsilon}{2\sqrt{Dt}}\right) - \operatorname{erfc}\left(\frac{x+h-\epsilon}{2\sqrt{Dt}}\right) + \sum_{n=1}^{\infty}\left\{\operatorname{erfc}\left(\frac{2nL+x-h+\epsilon}{2\sqrt{Dt}}\right) - \operatorname{erfc}\left(\frac{2nL+x+h+\epsilon}{2\sqrt{Dt}}\right) + \operatorname{erfc}\left(\frac{2nL-x-h-\epsilon}{2\sqrt{Dt}}\right) - \operatorname{erfc}\left(\frac{2nL-x+h-\epsilon}{2\sqrt{Dt}}\right)\right\}\right)\right] \quad (2)$$

where $\operatorname{erfc}(z) = 2\pi^{-1/2}\int_z^\infty e^{-\eta 2}\, d\eta$. The random walk simulations were also confirmed for particle diffusion in unobstructed 3-D space. For particles located initially at the origin.

$$C(x, y, z, t) = (2\pi Dt)^{-3/2} M e^{-(x^2+y^2+z^2)/4\,Dt} \quad (3)$$

RESULTS

Obstructed diffusion in mitochondria-like cylinders

Monte Carlo simulations were carried out to investigate 3-D diffusion in a closed cylinder with internal barriers. To confirm the accuracy of the random walk approach as used here, computations were first made for unobstructed diffusion in simple geometries in which analytical solution to the diffusion equation was possible. Diffusion was computed for a closed cylinder of length 200 lattice points and diameter 20 lattice points. Fig. 2 *A* shows the time evolution of particle concentration profile along the length of the cylinder in which the particles were located initially at a single plane at lattice point 50 (*diagrammed above graph*). The computed concentration profiles were compared to profiles determined by analytic solution of the diffusion equation for a finite cylinder with a delta function initial distribution (Eq. 1). The Monte Carlo simulation was in excellent agreement with the analytical solution (*smooth curves*). Time-resolved concentration profiles were also computed for initial particle distributions that simulated photobleaching experiments. For the computation in Fig. 2 *B*, the particles (representing bleached fluorophores) are located initially in a cylindrical segment of length 20 lattice points centered at lattice point 50. The concentration profiles computed by the random walk simulation agreed with the analytical solution to the diffusion equation for a square profile initial distribution (Eq. 2). Random walk simulations and analytical solutions also agreed for various other initial conditions and simple geometries, including open cylinder and unbounded 3-D space (not shown).

The effect of a single cristae-like barrier on particle diffusion in a closed cylinder was modeled. As seen for the random walk in Fig. 1 *A* (*bottom*) (particle position shown at every 10th time step), a particle encountering a barrier is hindered in its progress, and once past the barrier it is hindered from going back. To quantify the hindrance conferred by an obstacle on an ensemble of diffusing particles, Monte Carlo simulations were carried out for cylinders with single barriers occluding up to 93% of the lumen. Simulations in Fig. 3 were carried out for an initial square distribution of particles as in Fig. 2 *B*. Fig. 3 *A* shows the effect of an infinitely thin transverse barrier that occludes 77% of lumen cross-sectional area. The en face appearance of the barrier is that of an eyelid (shutter) without holes (other barrier shapes considered below). Compared to the concentration profiles for the same cylinder geometry and particle diffusion coefficient, but without barriers (Fig. 2 *B*), the barrier produced a slightly slowed decrease in particle concentration in the region initially occupied by the particles, and a slowed increase in concentration on the *trans* side of the barrier. At the barrier there was a discontinuity in concentration as particles "built up" at the *cis* barrier surface. The effects became more pronounced for a single

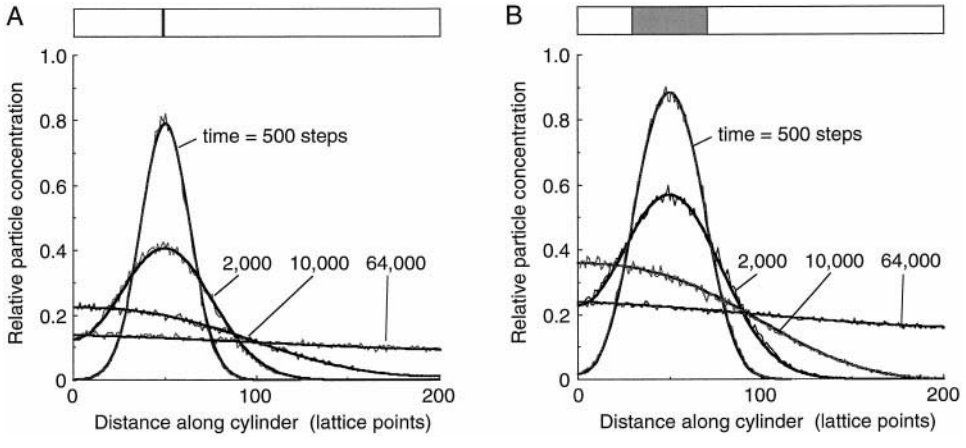

FIGURE 2 Comparison of analytic solutions for diffusion in an unobstructed closed cylinder (*smooth curves*) to random-walk Monte Carlo simulations in 3-D (*curves with noise*). Concentration profiles along the cylinder axis at the indicated number of time steps are shown for initial particle distributions confined to a plane (*A*, Eq. 1) or a volume corresponding to the bleach volume (*B*, Eq. 2). Simulations were done for 10^5 particles. $D = 0.16$ (lattice spacing)^2/time step for the analytical solution.

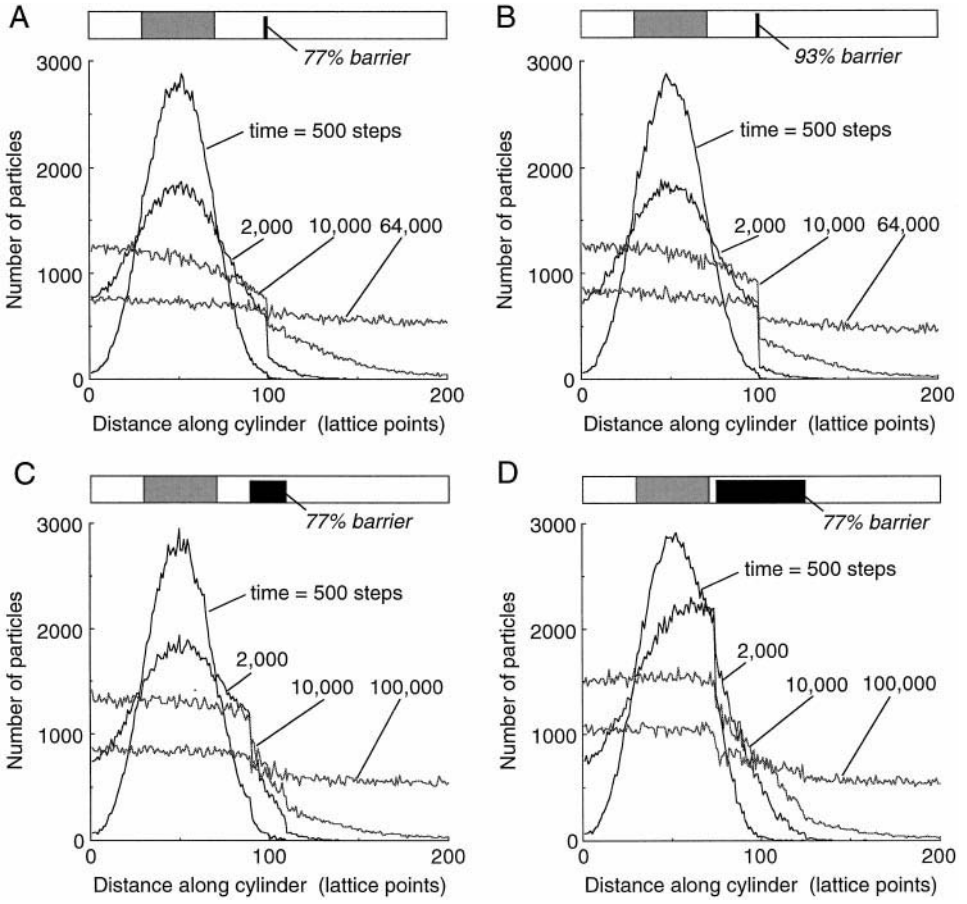

FIGURE 3 Time-resolved concentration profiles for single obstacles located at the center of a cylinder. Particles were initially located in a volume centered at lattice plane 50 and extending 20 lattice planes in each direction, as in Fig. 2 *B*. (*A*) Most (77%) of the plane in the center of the lumen is occluded by a thin (zero width) transverse barrier. (*B*) As in *A*, but with 93% of the plane occluded. (*C*) Most (77%) of the lumen is occluded by an obstacle of width 20 lattice planes centered at the middle of the cylinder. (*D*) As in *C*, but for a 77% obstacle of width 50 lattice planes.

thin barrier that occluded 93% of the cylinder lumen (Fig. 3 *B*). When the barriers were given nonzero width (20 and 50 lattice points, Fig. 3, *C* and *D*), apparent diffusion was slowed further. For these computations, the number of particles in the region of the barrier was corrected for the fractional volume occupied by the barrier.

To simulate spot photobleaching experiments, fluorescence recovery profiles were generated for different barriers by summing the number of particles in the bleach volume at each time. Because the bleach and probe volumes are generally the same in spot photobleaching experiments, the summation was performed over the length of the cylinder that initially contained the particles. Fig. 4 *A* shows computed photobleaching recovery curves (on a logarithmic time axis) for single barriers of different sizes and widths (as simulated in Fig. 3). As expected, the recovery rate was impeded by a barrier. There was a relatively minor effect on recovery curve shape at early times, when most particles did not diffuse far enough to encounter the barrier. However, an effect was seen at early times for the wide obstacle (50 lattice points), whose edge was near the initial location of particles. Barrier effects became apparent at late times, demonstrating that recovery curve shape is strongly dependent upon the nature of the barrier. This dependence of apparent diffusion coefficient on time defines an anomalous diffusion process (Nagle, 1992; Saxton, 1994; Feder et al., 1996). These results underscore the need to consider the curve shape of the full recovery in photobleaching studies of diffusion in obstructed environments. Often the percentage recovery at a single time such as the half-time ($t_{1/2}$) or the time for recovery to 75% of initial fluorescence ($t_{3/4}$) is used to deduce the diffusion coefficient. For the simulations here, the barriers (except for the wide barrier) would produce little effect on $t_{1/2}$, whereas apparent diffusion coefficients computed from $t_{3/4}$ would be decreased by 11% (77% thin obstacle), 22% (93% thin obstacle), 48% (77% obstacle, width 20 lattice points), and 81% (77% obstacle, width 50 lattice points).

Fig. 4 *B* demonstrates that the effect of fixed obstacles on diffusion is better appreciated by observing the depletion of fluorescence at a position far from the bleach zone. Fluorescence depletion curves were generated by summing the number of particles in a volume equivalent to the bleach volume, but centered around lattice point 180 on the *trans* side of the barrier. Barriers of increasing size and width produced a marked slowing of fluorescence depletion compared to that in the unobstructed cylinder.

Binding to the inner surface of the mitochondrion was considered to simulate metabolite binding to enzymes, or enzyme binding to a membrane-associated enzyme complex (Srere and Ovadi, 1990). Binding was modeled by forcing a particle that encounters the cylinder wall or an internal

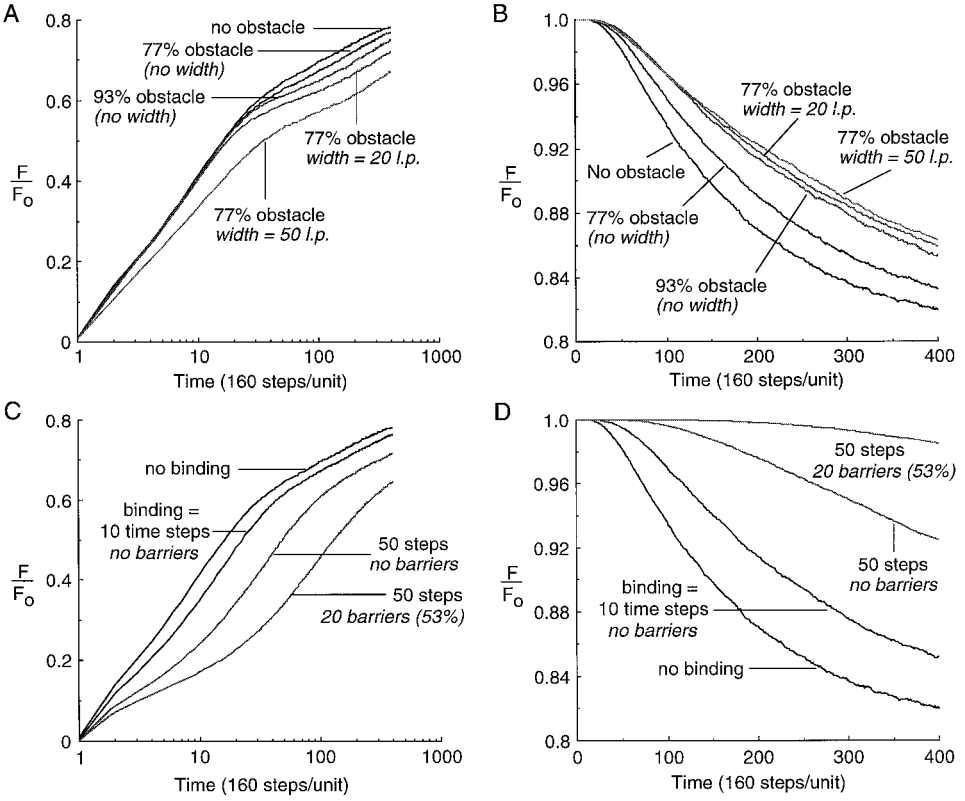

FIGURE 4 (*A*) Simulated fluorescence recovery curves for unobstructed diffusion in a cylinder (as in Fig. 2 *B*) and for the four single barrier geometries shown in Fig. 3. Fluorescence at indicated times relative to that before the bleach (F/F_o) was computed by summing the number of particles in the original bleach volume. At infinite time the fluorescence recovers to 80% of the original fluorescence ($F/F_o = 0.8$). Note that F/F_o in an actual photobleaching experiment would not drop to zero after a bleach pulse; however, the curve shape would be identical, except for a scaling factor related to bleach depth. Abbreviation: l.p., lattice points. (*B*) Simulated fluorescence depletion curves for the same set of barrier geometries. Fluorescence depletion curves were computed by summing the number of bleached fluorophore particles in a volume equal to the bleach volume, but centered at lattice plane 180. (*C*) Simulated fluorescence recovery curves for a cylinder in the presence of particle binding to the cylinder wall and barriers. The particle was kept in place for 10 and 50 time steps upon each encounter with a wall or barrier. Curves shown in the absence and presence of twenty 53% occluding barriers as indicated. (*D*) Simulated fluorescence depletion curves for the same binding and barrier parameters as in *C*.

barrier to remained fixed in place for a specified time (10 or 50 time steps). This is equivalent to specifying a kinetic zero-order unbinding rate, where the number of time steps for which the particle remains fixed is related to the mean residence time. The effect of binding on fluorescence recovery is shown in Fig. 4 *C*. Binding can produce a marked slowing of apparent diffusion. Based on 75% fluorescence recovery, the apparent diffusion coefficient in a closed cylinder without barriers was slowed by ~25% for mean residence time corresponding to 10 time steps, and by 75% for 50 time steps. It is noted that the recovery curve shape is relatively insensitive to binding except for scaling along the time axis. Therefore diffusion in the absence of obstacles appears nonanomalous, so that binding cannot easily be deduced from photobleaching measurements. Fig. 4 *C* also shows a marked slowing of apparent diffusion for binding in the presence of multiple obstacles (compare with Fig. 5 *B*; see below). Fig. 4 *D* shows the simulated fluorescence depletion curves corresponding to the binding/barrier parameters modeled in Fig. 4 *C*. Quite substantial effects on fluorescence depletion were found.

The barrier geometries modeled above consist en face of a continuous obstruction like an eyelid. To determine whether the planar barrier profile influences barrier efficacy in slowing diffusion, single thin barriers of different profiles were modeled. Each barrier was located at lattice point 100 and occluded 93% of the cross-sectional plane (294 of the 317 lattice points obstructed). Three distinct barrier profiles were evaluated: a continuous lid permitting particle passage near the cylinder wall (as modeled above), an annular barrier permitting particle passage near the center of the lumen, and a porous barrier containing multiple holes throughout the plane. Barrier profile had little effect on particle diffusion. Diffusion was increased by ~10% for the lid versus annular barrier, and was intermediate for the porous barrier (not shown). The minor increase in diffusion for the annular barrier probably arises because particles have a shorter average path to reach the opening at the center of the lumen than to reach the opening close to the cylinder wall. From these and related computations, it was concluded that for a constant fraction of occluded lumen area, the details of barrier profile have little influence on diffusion.

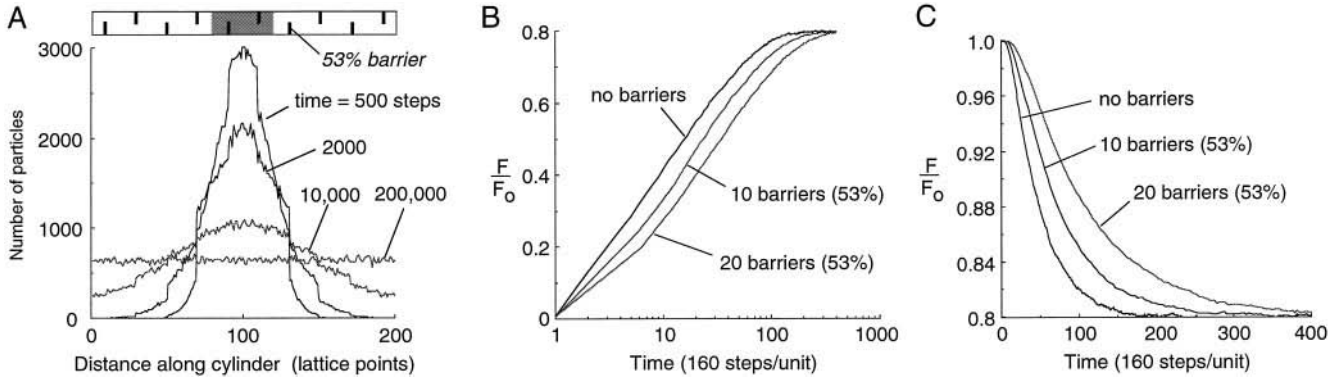

FIGURE 5 Diffusion in the presence of multiple barriers in series within a closed cylinder. Particles were located initially between lattice planes 80 and 120 (width 40). (*A*) Time-resolved concentration profiles for diffusion in a cylinder containing 20 equally spaced 53% barriers alternately occluding opposite halves of the cylinder lumen. (*B*) Fluorescence recovery curves for different numbers of 53% barriers. (*C*) Fluorescence depletion curves for same barrier geometries as in *B*; fluorescence was computed by summing the particles between lattice planes 80 and 120 at indicated times.

We next modeled 3-D diffusion in a closed cylinder containing a series of barriers (like mitochondrial cristae). As shown in the schematic at the top of Fig. 5 *A*, equally spaced thin barriers, each occluding 53% of the lumen, were alternately positioned at opposite sides of the cylinder lumen. The particles were located initially between two planes located 40 lattice points apart and centered at lattice point 100. Fig. 5 *A* shows the time evolution of axial particle concentration profile for the case of 10 barriers. The barriers produced a complex concentration profile and mildly slowed diffusion compared to diffusion in a cylinder without barriers. Fig. 5, *B* and *C*, shows simulated fluorescence recovery and depletion curves for 10 and 20 equally spaced barriers. Note the similarity in shape of recovery curves up to a time scaling factor. The apparent diffusion coefficient (defined by $t_{3/4}$) was decreased by 20% for 10 barriers, each occluding 53% of the lumen, and by 46% for 20 such barriers. The mild effect of multiple serial barriers on diffusion was an unexpected finding.

Diffusion in an endoplasmic reticulum-like network

Random walk simulations were carried out as described in Methods to investigate diffusion in a 3-D, ER-like network of cylinders. The reticulum was taken to be a three-dimensional orthogonal array of interconnected cylinders of specified diameter and spacing. To simulate photobleaching recovery experiments in cells, the array was taken to be infinite in extent in the *x*,*y* plane, but finite in the *z* direction. Photobleaching recovery curves were simulated for a bleach zone defined by the intersection of a cylinder of specified diameter with axis oriented in the *z* direction. Fig. 6 *A* shows time-resolved concentration profiles for unobstructed diffusion in a 3-D slab (*z* thickness 72 lattice points) in the absence of a reticulum. The cylindrical bleach beam of diameter 60 lattice points was directed along the *z* axis. Fig. 6 *B* shows diffusion in a region of the same thickness, but where particles were confined to the lumen of a reticular network of cylinders (diameter 10 lattice points, intercylinder spacing 34 lattice points). There was a relative minor effect on apparent particle diffusion of the reticulum that occluded 97% of 3-D space.

Fig. 6 *C* shows the fluorescence recovery for diffusion in reticula of different calibers and spacings (*curves b–f*; see legend for parameters) compared to that in unobstructed 3-D space (*curve a*). Recovery curve shapes were similar and in general did not have the same long tails for anomalous diffusion processes as for fixed obstructions. Using the $t_{3/4}$ for fluorescence recovery as an index of diffusion, it was found that diffusion was slowed by 39–60% for a wide range of reticular geometries occluding 90–97% of diffusive space. The fastest simulated fluorescence recovery (diffusion slowed by 39%) was seen for a reticulum of extent 3 lattice points in the *z* direction, equivalent to bleaching one sheet of cylinder reticulum in the *x*,*y* plane. Increasing the thickness of the reticulum to bleach 3 and 5 reticular sheets (72 and 140 l.p., *curves c and d*) slowed diffusion by 48% and 50% compared to free diffusion. Thus increasing the extent of the reticulum in the *z* direction had little effect on apparent particle diffusion. Similarly, changing intercylinder spacing and cylinder diameter had only minor effects on diffusive properties. Increasing the cylinder diameter from 3 to 7 lattice points (*curves c and f*) had no effect on $t_{3/4}$, each slowing apparent diffusion by ~48%. Changing the intercylindrical spacing from 14 to 34 lattice points also had minimal effect. As expected from the high surface-to-volume ratio of a reticulum, particle binding to the walls of the reticulum could produce a marked slowing of diffusion (*curve g*), with ~85% slowing when the mean residence time was 10 time steps. In terms of experimental strategies, photobleaching measurements of particle diffusion in the lumen of endoplasmic reticulum could provide a sensitive index of particle binding, such as that involved in interactions with the protein folding machinery.

Fig. 6 *D* shows simulations of fluorescence depletion in a reticular network for different distances between the observation volume and the original bleach volume. Because of

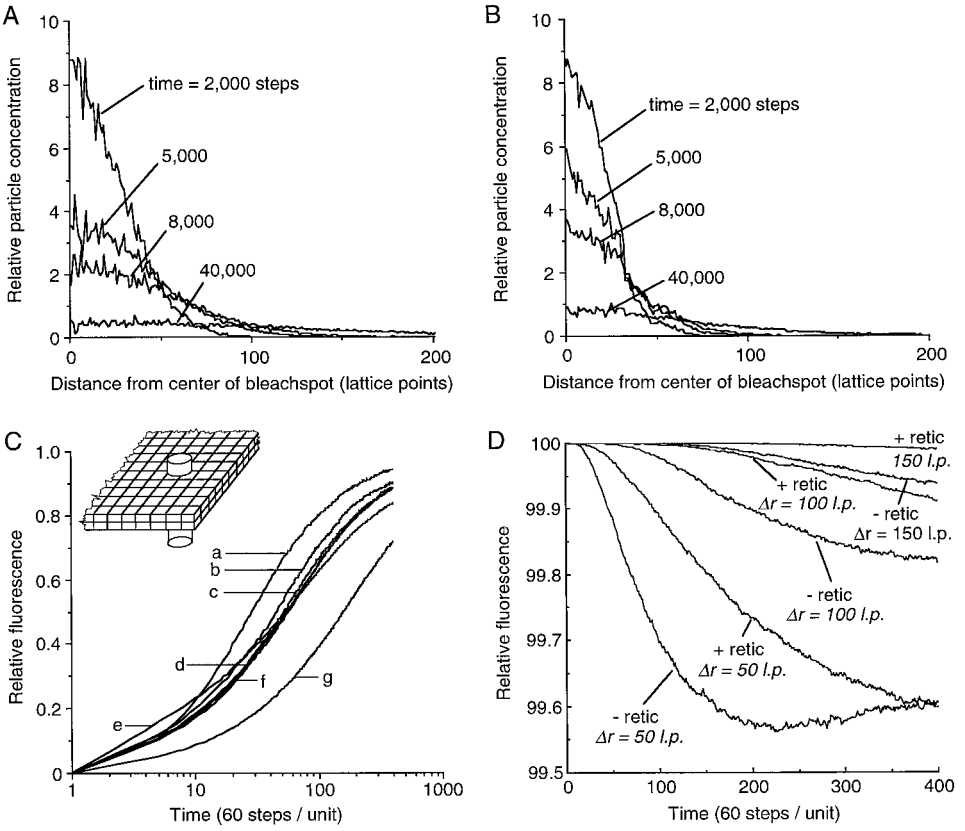

FIGURE 6 Diffusion in an endoplasmic reticulum-like 3-D orthogonal meshwork of interconnected cylinders. Particles were initially located in a cylindrical disk with a diameter of 60 lattice points (disk axis along z axis) and a z extent of 72 lattice points. Particles were confined to diffuse between infinite x-y planes at z lattice points 0 to 72. (*A*) Time evolution of particle concentration profile for diffusion in confined 3-D space without a reticulum. The ordinate is the relative concentration of particles at indicated cylinder radius from the z axis. Particles were summed over all z lattice points. (*B*) As in *A*, except that particles were confined to the continuously open lumen of a reticular network of cylinders with a diameter of 10 lattice points and an intercylinder axial spacing of 34 lattice points. (*C*) Photobleaching recovery curves in the absence and presence of reticula for different geometries, each with a bleach diameter of 60 lattice points (l.p.) in the absence (*a*) and presence (*b–g*) of a reticulum. (*b*) Cylinder diameter 3 l.p., cylinder spacing 34 l.p., z thickness 3 l.p. corresponding to one sheet of cylinder reticulum in the x-y plane. (*c*) Same as in *b*, but with z thickness corresponding to three sheets of cylinder reticulum in x, y (72 l.p.). (*d*) As in *b*, but with z thickness corresponding to five sheets of cylinder reticulum in x, y (140 l.p.). (*e*) As in *c*, but with cylinder spacing 14 l.p. (*f*) As in *c*, but cylinder diameter 7 l.p. (*g*) As in *c*, but with binding to the wall (10 time steps per interaction). See text for further explanation. (*D*) Fluorescence depletion curves in the presence or absence of a reticulum (as in *b* above) with indicated separation (Δr) between the axis of bleach beam and probed zone (of equal volume).

the infinite extent of the reticulum in the x,y plane, the fluorescence depletion signal decreases strongly as the distance between observation and bleach volumes increases. However, the curve shapes for fluorescence depletion at a given distance were fairly insensitive to the presence and detailed geometry of the reticulum (not shown). Note that fluorescence depletion curves have a biphasic shape, with an initial decrease followed by a slow increase to the original fluorescence. Thus the measurement of fluorescence depletion for analysis of particle diffusion in a reticulum is of limited usefulness.

DISCUSSION

The purpose of this computational study was to investigate aqueous-phase solute diffusion in cell organelles and to relate experimental photobleaching measurements to intrinsic diffusive rates. The computations took into account several of the complex geometric features of real organelles, including internal cristae-like barriers in mitochondria and the interconnected reticular network in endoplasmic reticulum. Solute binding to membrane surfaces was also modeled. After specifying an initial distribution of particles, random walk simulations were carried out to compute the time evolution of the spatial concentration profile. Fluorescence photobleaching recovery and depletion curves were simulated by spatial integration of concentration profiles over the probed volume. The computations established an approach to relating photobleaching data in organelles to solute diffusion coefficients, and revealed several unanticipated findings discussed below. A general paradigm emerging from this study is that organellar barriers must be quite severe to seriously impede solute diffusion.

There are several approaches to the computation of diffusive phenomena in complex 3-D geometries such as those in cellular organelles. Direct analytical solution of the dif-

fusion equation is in general very difficult, particularly for complex geometries and solute binding to surfaces. The finite-element method describes the dynamics of diffusion as time-dependent concentrations within distinct spatial elements by computation of diffusive solute fluxes across boundaries (Patankar, 1980). The boundary conditions specify the complex 3-D geometry. Application of the finite-element method is technically much more demanding than the random walk simulations reported here, particularly when many different geometries and binding phenomena are considered. The finite-element approach would be useful for tracking multiple interdependent variables, such as diffusion, ion drift, potentials, and chemical reaction (Schaff et al., 1997). The purpose of our study was to investigate the diffusion of independent particles in specified geometries without potentials or mobile obstacles. Random walk simulation by a Monte Carlo approach was used based on its simplicity and flexibility in defining geometry and binding. The accuracy of the Monte Carlo simulations was validated for simple geometries by demonstrating that time-dependent concentration profiles were identical to those computed by analytic solution of the diffusion equation. In addition, it was shown that increasing the spatial/time resolution of the computations did not affect the results. Thus, although it is computation intensive, the random walk method was readily adapted to complex mitochondrial and reticular geometries.

It was found that fluorescence recovery in a confined compartment with fixed barriers cannot be described by a single diffusion coefficient. The dependence of recovery curve shape on barrier geometry indicated anomalous diffusion, in which the apparent diffusion coefficient is time-dependent. In photobleaching measurements where fixed barriers may exist, it is thus important to obtain and analyze fluorescence recovery curves over sufficiently long times. The simulations reported here clearly demonstrate that determination of a single apparent diffusion coefficient from fluorescence recovery at a single time point can be seriously misleading. A potentially useful approach to addressing this concern is the analysis of fluorescence recovery curves in terms of a continuous distribution of diffusion coefficients and time-dependent diffusion coefficients. We recently developed a regression procedure using the Maximum Entropy Method to deduce diffusion coefficient distribution from photobleaching data (Periasamy et al., 1998). Preliminary analysis of experimental data for solute diffusion in the cytoplasm of living cells suggests that the concept of a diffusion coefficient distribution will be useful for describing diffusion in complex cellular compartments.

A motivation for carrying out the theoretical computations here was to interpret photobleaching recovery measurements of GFP diffusion in the mitochondrial matrix (Partikian et al., 1998). GFP was targeted to the aqueous phase of the mitochondrial matrix by transfection of cells with cDNA encoding a GFP-fusion protein containing the mitochondrial targeting presequence of COX8. Spot photobleaching recovery experiments done with a 100× objective (~0.8-μm spot diameter) indicated that the majority of the GFP was mobile and recovered with an apparent $t_{1/2}$ of 15–20 ms. The GFP diffusion coefficient was computed from the $t_{1/2}$ and a model of diffusion in unobstructed cylinders of mitochondrial size. The model took into account the bleaching of a random site along the mitochondrial axis, as well as a continuous distribution of mitochondrial orientations in 3-D. An important result from this study was that the computed diffusion coefficient for GFP (assuming an unobstructed mitochondrial lumen) was only about threefold lower than that in saline. The GFP diffusion coefficient would be higher if obstacles (cristae) were taken into account. The in vivo geometry of mitochondrial cristae is controversial because of artifacts associated with fixation for electron microscopy. The cristae have been depicted as thin obstructing barriers as in Fig. 1 *A*, as well as long strands traversing the width and length of mitochondria. The computations here indicate that multiple obstructions (comparable in number to those seen in electron micrographs of mitochondria) in series that each occlude 53% of the cylinder lumen have a fairly minor effect on measured recoveries in spot photobleaching experiments. Therefore the actual diffusion coefficient for GFP translational diffusion in mitochondrial matrix is probably not very different from that computed assuming an unobstructed matrix compartment. This result is reassuring, because GFP diffusion in the matrix cannot be faster than that in saline.

Another motivation for this computational study was to analyze molecular diffusion in the aqueous lumen of endoplasmic reticulum. We recently targeted GFP to ER by cell transfection with cDNA encoding GFP with a C-terminus KDEL sequence and an N-terminus preprolactin secretory signal peptide (Dayel and Verkman, 1998). In addition, various other GFP fusion proteins were constructed in which the fused moieties might interact with protein folding machinery located on the luminal membrane. It was found that GFP was mobile in the lumen of the endoplasmic reticulum, and that the mobility of GFP-fusion constructs could be modified by various maneuvers such as those affecting protein folding. The computations here establish a quantitative basis for relating the GFP diffusion coefficient to photobleaching data and for interpreting effects of binding on apparent diffusion. The computations indicate that apparent solute diffusion in a reticulum with continuously open lumen is not much slower than that in unobstructed 3-D space, but that solute binding to the lumen inner surface can profoundly slow diffusion.

The observation that particles executing a random walk have an uncanny ability to find sparsely distributed absorbing patches on the surface of a sphere was first recognized by Berg and Purcell (1977). Similar conclusions were reported for receptor binding, such as the diffusion of pheromones to receptors on the surface of moth antennae (Futrelle, 1982). The observation here that obstacles must be large to seriously impede diffusion in organellar geometries is in agreement with this earlier work. In qualititative terms, the diffusing particle "feels" its way along an obstacle to

locate a small opening, and then passes through the opening to escape to the opposite side.

Several recommendations emerge from these computations for experimental measurement of solute diffusion in organelles by photobleaching methods. Fluorescence recoveries should be measured over long times (ideally $>10^3\ t_{1/2}$) to reveal long tails indicative of anomalous diffusion, spatial heterogeneity in diffusive properties, and other complex kinetic phenomena. It is useful to measure the time course of fluorescence after photobleaching not only in the bleach volume, but at one or more points away from the bleach volume. Ideally, image analysis would provide the complete x,y (and z with confocal detection) profiles for analysis of barrier properties. Experimental maneuvers that affect solute binding to organelle walls and barriers, such as changes in pH, or in adduct identity in expressed GFP fusion proteins, can be extremely helpful. Maneuvers that alter organelle geometry, such as changes in oxidative/metabolic state in mitochondria leading to orthodox/condensed state transformations, and changes in Golgi geometry with brefeldin A, can also be useful. Finally, it should be mentioned that it is important in photobleaching studies to rule out recovery processes that are not related directly to solute translational diffusion, such as "reversible photobleaching" due to triplet state relaxation.

We thank Drs. M. Dayel, N. Periasamy, and M. Saxton for helpful advice and discussions.

This work was supported by grant DK43840 from the National Institutes of Health.

REFERENCES

Abney, J. R., B. Cutler, M. L. Fillbach, D. Axelrod, and B. A. Scalettar. 1997. Chromatin dynamics in interphase nuclei and its implications for nuclear structure. *J. Cell Biol.* 137:1459–1468.

Alexander, S. P., and C. L. Rieder. 1991. Chromosome motion during attachment to the vertebrate spindle: initial saltatory-like behavior of chromosomes and quantitative analysis of force production by nascent kinetochore fibers. *J. Cell Biol.* 113:805–815.

Berg, H. C., and E. M. Purcell. 1977. Physics of chemoreception. *Biophys. J.* 20:193–219.

Cole, N. B., C. L. Smith, N. Sciaky, M. Terasaki, M. Edidin, and J. Lippincott-Schwartz. 1996. Diffusional mobility of Golgi proteins in membranes of living cells. *Science.* 273:797–801.

Dayel, M., and A. S. Verkman. 1998. Diffusion of green fluorescent protein in the aqueous lumen of endoplasmic reticulum. *FASEB J.* (in press) (Abstr.).

DeGiorgi, F., M. Brini, C. Bastianutto, R. Marsault, M. Montero, P. Pizzo, R. Rozzi, and R. Rizzuto. 1996. Targeting aquorin and green fluorescent protein to intracellular organelles. *Gene.* 173:113–117.

Feder, T. J., I. Brust-Mascher, J. P. Slattery, B. Baird, and W. W. Webb. 1996. Constrained diffusion or immobile fraction on cell surfaces: a new interpretation. *Biophys. J.* 70:2367–2373.

Futrelle, R. F. 1982. Dictyostelium chemotactic response to spatial and temporal solute gradients. Theories of the limits of chemotactic sensitivity and of pseudochemotaxis. *J. Cell Biochem.* 18:197–212.

Halestrap, A. P. 1989. The regulation of the matrix volume of mammalian mitochondria in vivo and in vitro and its role in the control of mitochondrial metabolism. *Biochim. Biophys. Acta.* 973:355–382.

Kao, H. P., J. R. Abney, and A. S. Verkman. 1993. Determinants of the translational diffusion of a small solute in cytoplasm. *J. Cell Biol.* 120:175–184.

Lang, I., M. Scholz, R. Peters. 1986. Molecular mobility and nucleocytoplasmic flux in hepatoma cells. *J. Cell Biol.* 102:1183–1190.

Luby-Phelps, K., P. E. Castle, D. L. Taylor, and F. Lanni. 1987. Hindered diffusion of inert tracer particles in the cytoplasm of mouse 3T3 fibroblasts. *Proc. Natl. Acad. Sci. USA.* 84:4910–4913.

Nagle, J. F. 1992. Long tail kinetics in biophysics? *Biophys. J.* 63: 366–370.

Partikian, A., B. Ölveczky, R. Swaminathan, Y. Li, and A. S. Verkman. 1998. Rapid diffusion of green fluorescent protein in the mitochondrial matrix. *J. Cell Biol.* 140:821–829.

Patankar, S. V. 1980. Numerical Heat Transfer and Fluid Flow. Taylor and Francis, Washington, DC.

Periasamy, N., R. Swaminathan, and A. S. Verkman. 1998. Analysis of fluorophore diffusion in complex heterogeneous media and cell cytoplasm by continuous distributions of diffusion coefficients. *Biophys. J.* 74:A184. (Abstr.).

Press, W. H., S. A. Teulkolsky, W. T. Vellering, and B. P. Flannery. 1992. Numerical Recipes in C. Cambridge University Press, New York.

Rizzuto, R., M. Brini, P. Pizzo, M. Murgia, and T. Pozzan. 1995. Chimeric green fluorescent protein as a tool for visualizing subcellular organelles in living cells. *Curr. Biol.* 5:636–642.

Saxton, M. J. 1990. Lateral diffusion in a mixture of mobile and immobile particles: a Monte Carlo study. *Biophys. J.* 58:1303–1306.

Saxton, M. J. 1993. Lateral diffusion in an archipelago. Dependence on tracer size. *Biophys. J.* 64:1053–1062.

Saxton, M. J. 1994. Anomalous diffusion due to obstacles: a Monte Carlo study. *Biophys. J.* 66:394–401.

Scalettar, B. A., and J. R. Abney. 1991. Molecular crowding and protein diffusion in biological membranes. *Comm. Mol. Cell Biophys.* 7:79–107.

Schaff, J., C. C. Fink, B. Slepchenko, J. H. Carson, and L. M. Loew. 1997. A general computation framework for modeling cellular structure and function. *Biophys. J.* 73:1135–1146.

Schram, B., J. F. Tocanne, and A. Lopez. 1994. Influence of obstacles on lipid lateral diffusion: computer simulation of FRAP experiments and application to proteoliposomes and biomembranes. *Eur. Biophys. J.* 23:337–348.

Seksek, O., J. Biwersi, and A. S. Verkman. 1997. Translational diffusion of macromolecule-size solutes in cytoplasm and nucleus. *J. Cell. Biol.* 138:131–142.

Shelby, R. D., K. M. Hahn, and K.f. Sullivan. 1996. Dynamic elastic behavior of alpha-satellite DNA domains visualized in situ in living human cells. *J. Cell Biol.* 135:545–557.

Srere, P. A. 1980. The infrastructure of the mitochondrial matrix. *Trends Biochem. Sci.* 5:120–121.

Srere, P. A., and J. Ovadi. 1990. Enzyme-enzyme interactions and their metabolic role. A minireview. *FEBS Lett.* 268:360–367.

Swaminathan, R., C. P. Hoang, and A. S. Verkman. 1997. Photochemical properties of green fluorescent protein GFP-S65T in solution and transfected CHO cells: analysis of cytoplasmic viscosity by GFP translational and rotational diffusion. *Biophys. J.* 72:1900–1907.